RESEARCH ARTICLE | OCTOBER 02 2024

Phonon-assisted Auger decay of excitons in doped transition metal dichalcogenide monolayers

Special Collection: Festschrift in honor of Louis E. Brus

Benedikt Scharf ; Vasili Perebeinos

J. Chem. Phys. 161, 134709 (2024)
https://doi.org/10.1063/5.0230578
CHORUS

The Journal of Chemical Physics ARTICLE pubs.aip.org/aip/jcp

Phonon-assisted Auger decay of excitons in doped transition metal dichalcogenide monolayers

Cite as: J. Chem. Phys. 161, 134709 (2024); doi: 10.1063/5.0230578
Submitted: 24 July 2024 • Accepted: 18 September 2024 •
Published Online: 2 October 2024

Benedikt Scharf[1] and Vasili Perebeinos[2,a)]

AFFILIATIONS

[1] Institute for Theoretical Physics and Astrophysics and Würzburg-Dresden Cluster of Excellence ct.qmats, University of Würzburg, Am Hubland, 97074 Würzburg, Germany
[2] Department of Electrical Engineering, University at Buffalo, Buffalo, New York 14228, USA

Note: This paper is part of the JCP Festschrift in Honor of Louis E. Brus.
[a)] **Author to whom correspondence should be addressed:** vasilipe@buffalo.edu

ABSTRACT

The competition between the radiative and nonradiative lifetimes determines the optical quantum yield and plays a crucial role in the potential optoelectronic applications of transition metal dichalcogenides (TMDCs). Here, we show that, in the presence of free carriers, an additional nonradiative decay channel opens for excitons in TMDC monolayers. Although the usual Auger decay channel is suppressed at low doping levels by the simultaneous momentum and energy conservation laws, exciton–phonon coupling relaxes this suppression. By solving a Bethe–Salpeter equation, we calculate the phonon-assisted Auger decay rates in four typical TMDCs as a function of doping, temperature, and dielectric environment. We find that even for a relatively low doping of 10^{12} cm^{-2}, the nonradiative lifetime ranges from 16 to 165 ps in different TMDCs, offering competition to the radiative decay channel.

I. INTRODUCTION

The exceptional properties exhibited by two-dimensional (2D) materials have revolutionized the landscape of materials science and nanotechnology.[1,2] The interplay between radiative and nonradiative recombination processes in transition metal dichalcogenides (TMDCs) is fundamental to their optoelectronic properties.[3–5] These two-dimensional semiconductors exhibit strong light–matter interactions,[6] making them promising candidates for various photonic and optoelectronic applications.[7] The optical quantum yield,[8,9] a critical parameter for such applications, is directly influenced by the competition between the radiative[10–13] and nonradiative[14] exciton lifetimes.[15,16]

In TMDC monolayers, excitons, or bound electron–hole pairs, play a crucial role in determining the material's optical properties.[17–20] The radiative recombination of these excitons results in photon emission, which contributes to the material's luminescence. However, nonradiative recombination pathways can significantly impact the overall quantum efficiency of these materials.[21] Therefore, understanding these dynamics is crucial for optimizing TMDC-based devices for various optoelectronic applications.[3,4]

In this work, we demonstrate that the nonradiative exciton–phonon-assisted Auger decay channel can effectively compete with the radiative decay even at moderately low doping levels, especially in smaller bandgap TMDCs. The conventional Auger decay mechanism, a nonradiative process often observed in semiconductors,[22–24] is suppressed in TMDC monolayers at low doping concentrations. This suppression is attributed to the simultaneous conservation of momentum and energy in these 2D systems. However, phonon emission or absorption can relax momentum conservation, enabling phonon-assisted Auger decay of excitons available even at low doping levels.[25] The Auger decay with phonon assistance has been considered in bulk semiconductors.[26] In this work, we extend the phonon-assisted Auger decay mechanism to strongly bound excitons in 2D van der Waals materials. Strong exciton–phonon coupling in TMDCs[27–29] is responsible, for example, for the temperature-dependent width of

photoluminescent spectra[30–37] and magneto-optical spectroscopy[38] and provides new possibilities for ultrafast intralayer-to-interlayer exciton transitions and interlayer charge transfer.[39]

II. METHODS AND MODEL

We use standard notations throughout this paper, where $e > 0$ stands for the elementary charge, ε_0 is the vacuum permittivity, and k_B is the Boltzmann constant.

A. Excitons

To compute the phonon-assisted Auger decay rate for excitons in TMDCs, we first obtain the single-particle spectrum from the model tight-binding Hamiltonian derived in Ref. 40. Within the tight-binding model, a given single-particle state $|n\boldsymbol{k}\rangle$ with wave vector $\boldsymbol{k}$ in band n and energy $\varepsilon_{n\boldsymbol{k}}$ can be written as the Bloch sum,

$$|n\boldsymbol{k}\rangle = \frac{1}{\sqrt{N}}\sum_{\nu,\boldsymbol{R}} e^{\imath \boldsymbol{k}\cdot\boldsymbol{R}} a_{n\boldsymbol{k}\nu}|\nu,\boldsymbol{R}\rangle, \tag{1}$$

where $|\nu,\boldsymbol{R}\rangle$ is the orbital ν centered at the Bravais lattice point $\boldsymbol{R}$ and N is the total number of primitive unit cells considered. The coefficients $a_{n\boldsymbol{k}\nu}$ in Eq. (1) are determined from the tight-binding Hamiltonian via

$$\sum_{\nu'} \mathscr{H}_{\nu\nu'}(\boldsymbol{k}) a_{n\boldsymbol{k}\nu'} = \varepsilon_{n\boldsymbol{k}} a_{n\boldsymbol{k}\nu}, \tag{2}$$

where the 11-band tight-binding Hamiltonian $\mathscr{H}_{\nu\nu'}$ and its corresponding hopping parameters are taken from Ref. 40. For simplicity, we use the 11-band model without spin–orbit coupling in the remainder of this work.

The tight-binding states determined from Eqs. (1) and (2) are then used to compute the exciton dispersion via a Bethe–Salpeter equation (BSE). For an exciton S with momentum $\boldsymbol{q}$, this BSE can be conveniently written as[41,42]

$$\begin{aligned}&[\Omega_S(\boldsymbol{q}) - \varepsilon_c(\boldsymbol{k}+\boldsymbol{q}) + \varepsilon_v(\boldsymbol{k})]\mathscr{A}^{S\boldsymbol{q}}_{vc\boldsymbol{k}} \\ &\quad = \sum_{v'c'\boldsymbol{k}'} \left[\mathscr{K}^{\mathrm{d}}_{vc\boldsymbol{k},v'c'\boldsymbol{k}'}(\boldsymbol{q}) + \mathscr{K}^{\mathrm{x}}_{vc\boldsymbol{k},v'c'\boldsymbol{k}'}(\boldsymbol{q})\right]\mathscr{A}^{S\boldsymbol{q}}_{v'c'\boldsymbol{k}'},\end{aligned} \tag{3}$$

where $\Omega_S(\boldsymbol{q})$ denotes the exciton energy and $\mathscr{A}^{S\boldsymbol{q}}_{vc\boldsymbol{k}}$ denote the coefficients of the linear combination forming the excitonic state,

$$|\Psi_{S\boldsymbol{q}}\rangle = \sum_{vc\boldsymbol{k}} \mathscr{A}^{S\boldsymbol{q}}_{vc\boldsymbol{k}} \hat{c}^\dagger_{c\boldsymbol{k}+\boldsymbol{q}}\hat{c}_{v\boldsymbol{k}}|\mathrm{GS}\rangle \equiv \hat{X}^\dagger_{S\boldsymbol{q}}|\mathrm{GS}\rangle. \tag{4}$$

Here, $\hat{c}^\dagger_{c\boldsymbol{k}}$ ($\hat{c}_{v\boldsymbol{k}}$) is the creation (annihilation) operator of an electron with momentum $\boldsymbol{k}$ in a conduction band c (valence band v) and $|\mathrm{GS}\rangle$ is the ground state with fully occupied valence bands and unoccupied conduction bands, while $\hat{X}^\dagger_{S\boldsymbol{q}}$ is the creation operator of an exciton in state S with momentum $\boldsymbol{q}$. Equation (3) contains the direct and exchange terms

$$\mathscr{K}^{\mathrm{d}}_{vc\boldsymbol{k},v'c'\boldsymbol{k}'}(\boldsymbol{q}) = -\sum_{\nu\nu'} a^*_{c\boldsymbol{k}+\boldsymbol{q}\nu} a_{c'\boldsymbol{k}'+\boldsymbol{q}\nu} a_{v\boldsymbol{k}\nu'} a^*_{v'\boldsymbol{k}'\nu'} \times \left[\frac{1}{N}\sum_{\boldsymbol{R}} e^{-\imath(\boldsymbol{k}-\boldsymbol{k}')\cdot\boldsymbol{R}} W(|\boldsymbol{R}|)\right] \tag{5}$$

and

$$\mathscr{K}^{\mathrm{x}}_{vc\boldsymbol{k},v'c'\boldsymbol{k}'}(\boldsymbol{q}) = \sum_{\nu\nu'} a^*_{c\boldsymbol{k}+\boldsymbol{q}\nu} a_{v\boldsymbol{k}\nu} a_{c'\boldsymbol{k}'+\boldsymbol{q}\nu'} a^*_{v'\boldsymbol{k}'\nu'} \left[\frac{1}{N}\sum_{\boldsymbol{R}} e^{-\imath\boldsymbol{q}\cdot\boldsymbol{R}} V(|\boldsymbol{R}|)\right], \tag{6}$$

respectively. Equations (5) and (6) have been derived assuming point-like orbitals. The direct and exchange terms are computed in the real space from the screened interaction and the bare Coulomb potentials $W(|\boldsymbol{R}|)$ and $V(|\boldsymbol{R}|)$, respectively. If we do not account for doping in the BSE, $W(|\boldsymbol{R}|) = V(|\boldsymbol{R}|)$. In 2D materials, this potential can be well modeled by the Keldysh potential,[43–45]

$$W(|\boldsymbol{R}|) = \frac{e^2}{8\varepsilon_0 r_0}\left[H_0\left(\frac{\kappa|\boldsymbol{R}|}{r_0}\right) - Y_0\left(\frac{\kappa|\boldsymbol{R}|}{r_0}\right)\right], \tag{7}$$

where H_0 is the Struve function, Y_0 is the Bessel function of the second kind, ε_0 is the vacuum permittivity, κ is the averaged relative permittivity of the dielectric background,[46] and r_0 is the monolayer polarizability parameter.

B. Phonon-assisted Auger decay rate

Having obtained $\Omega_S(\boldsymbol{q})$ and $\mathscr{A}^{S\boldsymbol{q}}_{vc\boldsymbol{k}}$ from Eq. (3), we are now in a position to compute the phonon-assisted Auger scattering rate.

In the second-order processes we consider (see Fig. 1), the initial state is given by a zero-momentum exciton and an electron with momentum $\boldsymbol{k}'$ in the lowest conduction band c_0. By emitting a phonon with momentum $-\boldsymbol{q}$ or absorbing a phonon with momentum $\boldsymbol{q}$, the exciton acquires a finite momentum $\boldsymbol{q}$. This intermediate state, in turn, collapses to the final state by Auger decay of the exciton to the ground state. The energy conservation then requires $\Omega_S(\boldsymbol{0}) + \varepsilon_{c_0\boldsymbol{k}'} = \hbar\omega_{-\boldsymbol{q}} + \varepsilon_{c'\boldsymbol{k}'+\boldsymbol{q}}$ for phonon emission and $\Omega_S(\boldsymbol{0}) + \varepsilon_{c_0\boldsymbol{k}'} + \hbar\omega_{\boldsymbol{q}} = \varepsilon_{c'\boldsymbol{k}'+\boldsymbol{q}}$ for phonon absorption, where $\hbar\omega_{\pm\boldsymbol{q}}$ is the phonon dispersion and $\varepsilon_{c\boldsymbol{k}}$ is the electron dispersion in a conduction band c. During the transition to the final state, we allow for excitations to an arbitrary conduction band c', that is, not only within the lowest conduction band c_0 [Fig. 1(b) shows only one conduction band for simplicity].

We model the interaction mediating the collapse from the initial state to the final state by the Hamiltonian $\hat{H} = \hat{H}_{\mathrm{e-ph}} + \hat{H}_{\mathrm{e-e}}$ with the exciton–phonon interaction,

$$\hat{H}_{\mathrm{e-ph}} = \frac{g}{\sqrt{N}}\sum_{S\boldsymbol{k}\boldsymbol{q}} \hat{X}^\dagger_{S\boldsymbol{k}+\boldsymbol{q}}\hat{X}_{S\boldsymbol{k}}\left(\hat{b}^\dagger_{-\boldsymbol{q}} + \hat{b}_{\boldsymbol{q}}\right), \tag{8}$$

and the electron–electron interaction,

$$\hat{H}_{\mathrm{e-e}} = \frac{1}{N}\sum_{cc'v\boldsymbol{k}\boldsymbol{k}'\boldsymbol{q}} U^{c',c_0,c,v}_{\boldsymbol{k}'+\boldsymbol{q},\boldsymbol{k}',\boldsymbol{k}+\boldsymbol{q},\boldsymbol{k}} \hat{c}^\dagger_{c'\boldsymbol{k}'+\boldsymbol{q}}\hat{c}_{c_0\boldsymbol{k}'}\hat{c}_{c\boldsymbol{k}+\boldsymbol{q}}\hat{c}^\dagger_{v\boldsymbol{k}}. \tag{9}$$

Equation (8) contains the exciton creation (annihilation) operator $\hat{X}^\dagger_{S\boldsymbol{k}}$ ($\hat{X}_{S\boldsymbol{k}}$) defined in Eq. (4). In our model, the exciton–phonon

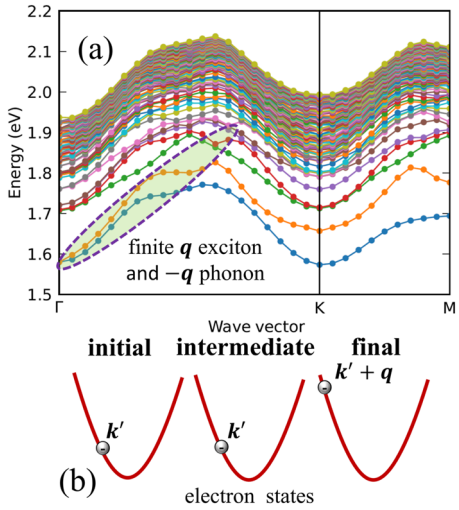

FIG. 1. Phonon-assisted Auger decay mechanism. (a) Exciton dispersion of $MoSe_2$ as a function of the center-of-mass momentum evaluated on a $60 \times 60k$-mesh of the Brillouin zone. Only the first 100 exciton bands are shown. The onset of the single-particle continuum at $q = 0$ takes place at an energy of 1.89 eV. The colored oval demonstrates the transition of the zero-momentum exciton to a finite q-exciton by emission of a phonon with momentum $-\boldsymbol{q}$ in the intermediate state. (b) Electron states in the phonon-assisted Auger decay process: An initial state comprising a zero-momentum exciton and a conduction band electron with momentum $\boldsymbol{k}'$ is excited by emission (absorption) of a phonon with momentum $-\boldsymbol{q}$ ($\boldsymbol{q}$) into an intermediate state comprising an exciton with finite momentum $\boldsymbol{q}$ and the conduction band electron $\boldsymbol{k}'$. In the final state, the $\boldsymbol{q}$-exciton decays into the ground state by an Auger process and transfers its momentum to the conduction band electron.

coupling strength in Eq. (8) is given by a constant g, while the Auger Coulomb matrix element in Eq. (9) is given by

$$U^{c',c_0,c,v}_{\boldsymbol{k}'+\boldsymbol{q},\boldsymbol{k}',\boldsymbol{k}+\boldsymbol{q},\boldsymbol{k}} = \sum_{vv'} a^*_{c'\boldsymbol{k}'+\boldsymbol{q}v} a_{c\boldsymbol{k}+\boldsymbol{q}v} a_{c_0\boldsymbol{k}'v'} a^*_{v\boldsymbol{k}v'} \left[\frac{1}{N}\sum_{\boldsymbol{R}} e^{-i(\boldsymbol{k}'-\boldsymbol{k})\cdot\boldsymbol{R}} V(|\boldsymbol{R}|)\right]. \tag{10}$$

Here, Eq. (10) has been calculated employing the same approximations as those used to arrive at Eqs. (5) and (6).

Using second order perturbation theory and Fermi's golden rule, we can determine the Auger scattering rate as

$$\begin{aligned}\frac{\hbar}{\tau} = {} & \frac{2\pi g^2}{N^3}\sum_{c',\boldsymbol{k}',S,\boldsymbol{q}} \frac{\left|\sum_{c\boldsymbol{k}} \mathscr{A}^{S\boldsymbol{q}}_{v\boldsymbol{c}\boldsymbol{k}} U^{c',c_0,c,v}_{\boldsymbol{k}'+\boldsymbol{q},\boldsymbol{k}',\boldsymbol{k}+\boldsymbol{q},\boldsymbol{k}}\right|^2}{\left[\Omega_S(\boldsymbol{q}) - \Omega_S(\boldsymbol{0}) + \hbar\omega_{-\boldsymbol{q}}\right]^2} \\ & \times f(\varepsilon_{c_0\boldsymbol{k}'})\left[1 - f(\varepsilon_{c'\boldsymbol{k}'+\boldsymbol{q}})\right]\left[1 + n_{-q}\right] \\ & \times \delta\left[\varepsilon_{c'\boldsymbol{k}'+\boldsymbol{q}} - \varepsilon_{c_0\boldsymbol{k}'} + \hbar\omega_{-\boldsymbol{q}} - \Omega_S(\boldsymbol{0})\right] \\ & + \frac{2\pi g^2}{N^3}\sum_{c',\boldsymbol{k}',S,\boldsymbol{q}} \frac{\left|\sum_{c\boldsymbol{k}} \mathscr{A}^{S\boldsymbol{q}}_{v\boldsymbol{c}\boldsymbol{k}} U^{c',c_0,c,v}_{\boldsymbol{k}'+\boldsymbol{q},\boldsymbol{k}',\boldsymbol{k}+\boldsymbol{q},\boldsymbol{k}}\right|^2}{\left[\Omega_S(\boldsymbol{q}) - \Omega_S(\boldsymbol{0}) - \hbar\omega_{\boldsymbol{q}}\right]^2} \\ & \times f(\varepsilon_{c_0\boldsymbol{k}'})\left[1 - f(\varepsilon_{c'\boldsymbol{k}'+\boldsymbol{q}})\right] n_q \\ & \times \delta\left[\varepsilon_{c'\boldsymbol{k}'+\boldsymbol{q}} - \varepsilon_{c_0\boldsymbol{k}'} - \hbar\omega_{\boldsymbol{q}} - \Omega_S(\boldsymbol{0})\right], \end{aligned} \tag{11}$$

where the first and second terms are the contributions due to phonon emission and absorption, respectively. The integral over $1/x^2$ in Eq. (11) should be evaluated as a principal part, that is, $1/x^2 \to [1 - \exp(-x^2/\sigma^2)]/x^2$, where the value of σ depends on the k-mesh. Here, we use $\sigma = 50$ meV and a 60×60 k-mesh. The functions

$$f(\varepsilon) = \frac{1}{\exp\left[(\varepsilon - \mu)/k_B T\right] + 1}, n_{\boldsymbol{q}} = \frac{1}{\exp\left(\hbar\omega_{\boldsymbol{q}}/k_B T\right) - 1} \tag{12}$$

denote the Fermi–Dirac and Bose–Einstein distribution functions with temperature T and chemical potential μ. In order to obtain Eq. (11), we have assumed that only the lowest conduction band c_0 is occupied by excess electrons[47] and that phonon-assisted transitions can occur only between this band and any other conduction band.

C. Exciton–phonon coupling strength

To estimate the strength of the exciton–phonon coupling, we use the experimentally measured full-width at half-maximum γ from temperature-dependent photoluminescence spectra (shown in Fig. 2) according to Fermi's golden rule,

$$\gamma(T) = \gamma_0 + 2\pi g^2 DOS_{exc} n_{ph}, \tag{13}$$

where γ_0 is a temperature-independent broadening due to defects and sample inhomogeneities and the temperature dependence arises from the phonon population n_{ph} according to Eq. (12). The exciton density of states is evaluated according to $DOS_{exc} = m_{exc}A/(2\pi\hbar^2)$, where A is the area of the primitive unit cell, and the exciton mass $m_{exc} = m_c + m_v$ is given by the sum of conduction and valence band effective masses from Table I. The values of g from the best fits are given in Table I. Note that we only consider phonon absorption in Eq. (13), since there are no states to scatter to as a result of the phonon emission for the lowest-energy excitons and we do not differentiate between acoustic and optical phonon contributions to the full-width at half maximum by using a fixed value of the phonon energy of $\hbar\omega_{ph} = 20$ meV for all TMDCs considered in Eqs. (11) and (13). Note that we use a momentum- and band-independent approximation for the strength of the exciton–phonon coupling, which is in the spirit of the commonly used deformation potential approximation in the context of electrical transport. The deformation potential approximation is justifiable because of the weak dependence of the coupling between electrons and optical non-polar phonons. We also employ the Einstein model for the optical phonons, that is, a momentum-independent phonon energy. Since the parameters of our model are obtained by refitting the existing experimental data on phonon-induced broadening of photoluminescence spectra, we expect that those are quantitative results, which are comparable with future experiments.

III. RESULTS

Equations (2)–(13) can then be used to compute the phonon-assisted Auger decay rate. Here, we present the results for four different TMDCs, namely MoS_2, $MoSe_2$, WS_2, and WSe_2. As shown

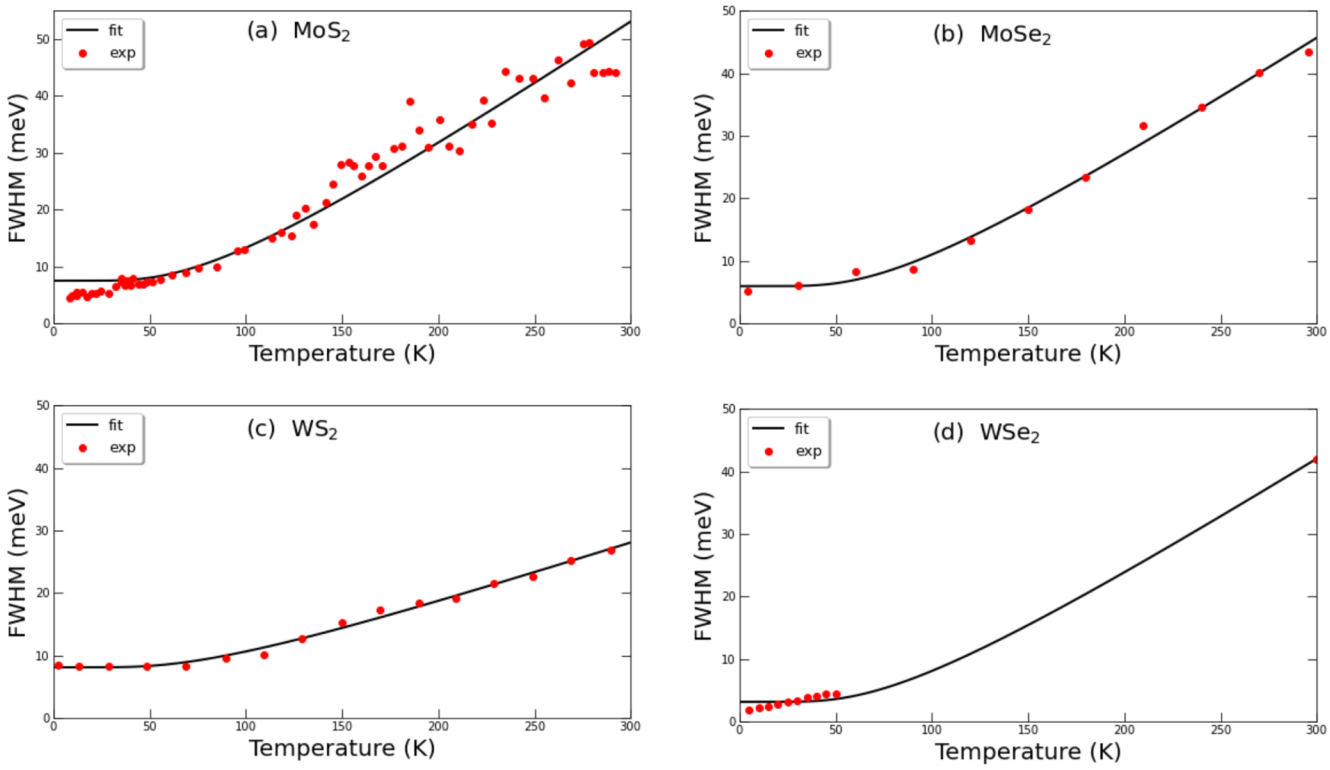

FIG. 2. Full-width at half maximum data analysis of (a) MoS_2,[30] (b) $MoSe_2$,[31] (c) WS_2,[32] and (d) WSe_2[33,36] to extract the corresponding strengths of the exciton–phonon coupling according to fits to Eq. (13).

in Fig. 3, for all four TMDCs, the scattering rates for the process considered in this work increase with doping densities and correspond to lifetimes in the sub-nanosecond regime at densities up to 10^{13} cm^{-2}.

In systems with strong dielectric screening, on the other hand, the phonon-assisted Auger scattering rate is suppressed, as illustrated in Fig. 4: The stronger the dielectric screening, the smaller the Auger scattering rate. In the limit of an infinitely large dielectric constant, the phonon-assisted exciton Auger decay rate vanishes as shown in Fig. 4 containing data computed from Eq. (11) along with an empirical fit.

TABLE I. Effective masses of the lowest conduction band and the uppermost valence band in units of the free electron mass m_0 (taken from Ref. 40). The primitive unit cell area is given by $A = a^2\sqrt{3}/2$, where a is the lattice constant. The best-fit values of the exciton–phonon coupling g to Eq. (13) are also given in the last column.

Material	m_c/m_0	m_v/m_0	a (Å)	g (eV)
MoS_2	0.47	0.57	3.18	0.211
$MoSe_2$	0.54	0.65	3.32	0.176
WS_2	0.31	0.41	3.18	0.168
WSe_2	0.34	0.44	3.32	0.216

The temperature dependence follows from the probabilities of phonon emission and absorption, that is, $1 + 2n_{ph}$. The overall rate depends sensitively on the bandgap of the TMDCs, that is, the smaller the bandgap, the stronger the phonon-assisted exciton Auger decay rate. To probe the proposed phonon-assisted exciton

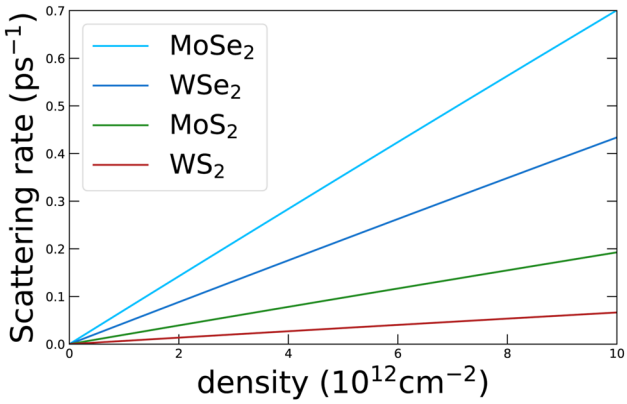

FIG. 3. Phonon-assisted Auger decay rate of excitons in four most common TMDC monolayers as a function of doping, evaluated at $T = 300$ K and in a dielectric environment $\kappa = 3$.

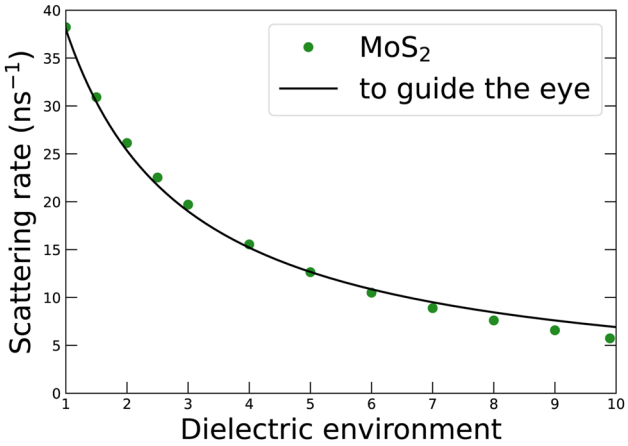

FIG. 4. Phonon-assisted Auger decay rate of excitons in MoS_2 as a function dielectric constant of the environment, evaluated at the doping level of 10^{12} cm^{-2} and at $T = 300$ K. The "to guide the eye" curve, $\propto 1/(1+\kappa)$, demonstrates vanishing scattering rate in the limit of $\kappa \to \infty$.

Auger decay mechanism, we want the experimental sample to be free of defects to limit other nonradiative defect-assisted decay channels. The gate can supply the free carrier in a TMDC in a controllable way such that the measured phonon-assisted exciton Auger decay rate could be analyzed according to the following empirical formula:

$$\frac{1}{\tau} = \frac{1+2n_{ph}}{\tau_0}\frac{\rho}{\rho_0}\frac{\kappa_0+1}{\kappa+1}, \tag{14}$$

where τ_0 is the phonon-assisted exciton Auger decay lifetime measured at typical experimentally relevant conditions, that is, $\rho_0 = 10^{12}$ cm^{-2}, $\kappa_0 = 3$, and $T = 4$ K. The value of τ_0 falls in the range of 16–165 ps depending on the bandgap of the TMDC material.

IV. CONCLUSIONS

We have demonstrated that the phonon-assisted exciton Auger decay mechanism can effectively compete with the radiative decay channel in defect-free samples, even at moderately low doping levels. The predicted values of the phonon-assisted Auger lifetime for excitons under typical experimental conditions are predicted to be in the range of 16–165 ps depending on the bandgap of the TMDC material. We believe that our work will stimulate further experimental work.

ACKNOWLEDGMENTS

We gratefully acknowledge the support by the National Science Foundation under Grant No. 2230727 and the computational facilities at the Center for Computational Research at the University at Buffalo (http://hdl.handle.net/10477/79221).

AUTHOR DECLARATIONS

Conflict of Interest

The authors have no conflicts to disclose.

Author Contributions

Benedikt Scharf: Conceptualization (equal); Data curation (equal); Writing – original draft (equal); Writing – review & editing (equal). **Vasili Perebeinos**: Conceptualization (equal); Data curation (equal); Writing – original draft (equal); Writing – review & editing (equal).

DATA AVAILABILITY

The data that support the findings of this study are available from the corresponding author upon reasonable request.

REFERENCES

[1]K. S. Novoselov, A. Mishchenko, A. Carvalho, and A. H. Castro Neto, "2D materials and van der Waals heterostructures," Science **353**, aac9439 (2016).
[2]S. Manzeli, D. Ovchinnikov, D. Pasquier, O. V. Yazyev, and A. Kis, "2D transition metal dichalcogenides," Nat. Rev. Mater. **2**, 17033 (2017).
[3]Q. H. Wang, K. Kalantar-Zadeh, A. Kis, J. N. Coleman, and M. S. Strano, "Electronics and optoelectronics of two-dimensional transition metal dichalcogenides," Nat. Nanotechnol. **7**, 699 (2012).
[4]K. F. Mak and J. Shan, "Photonics and optoelectronics of 2D semiconductor transition metal dichalcogenides," Nat. Photonics **10**, 216 (2016).
[5]A. Pospischil and T. Mueller, "Optoelectronic devices based on atomically thin transition metal dichalcogenides," Appl. Sci. **6**, 78 (2016).
[6]L. Britnell, R. M. Ribeiro, A. Eckmann, R. Jalil, B. D. Belle, A. Mishchenko, Y.-J. Kim, R. V. Gorbachev, T. Georgiou, S. V. Morozov, A. N. Grigorenko, A. K. Geim, C. Casiraghi, A. H. C. Neto, and K. S. Novoselov, "Strong light-matter interactions in heterostructures of atomically thin films," Science **340**, 1311–1314 (2013).
[7]L. Huang, A. Krasnok, A. Alú, Y. Yu, D. Neshev, and A. E. Miroshnichenko, "Enhanced light–matter interaction in two-dimensional transition metal dichalcogenides," Rep. Prog. Phys. **85**, 046401 (2022).
[8]M. Amani, D.-H. Lien, D. Kiriya, J. Xiao, A. Azcatl, J. Noh, S. R. Madhvapathy, R. Addou, S. Kc, M. Dubey, K. Cho, R. M. Wallace, S.-C. Lee, J.-H. He, J. W. Ager III, X. Zhang, E. Yablonovitch, and A. Javey, "Near-unity photoluminescence quantum yield in MoS_2," Science **350**, 1065–1068 (2015).
[9]Y. Lee, J. D. S. Forte, A. Chaves, A. Kumar, T. T. Tran, Y. Kim, S. Roy, T. Taniguchi, K. Watanabe, A. Chernikov, J. I. Jang, T. Low, and J. Kim, "Boosting quantum yields in two-dimensional semiconductors via proximal metal plates," Nat. Commun. **12**, 7095 (2021).
[10]M. Palummo, M. Bernardi, and J. C. Grossman, "Exciton radiative lifetimes in two-dimensional transition metal dichalcogenides," Nano Lett. **15**, 2794–2800 (2015).
[11]H. Liu, T. Wang, C. Wang, D. Liu, and J. Luo, "Exciton radiative recombination dynamics and nonradiative energy transfer in two-dimensional transition-metal dichalcogenides," J. Phys. Chem. C **123**, 10087–10093 (2019).
[12]C. Robert, D. Lagarde, F. Cadiz, G. Wang, B. Lassagne, T. Amand, A. Balocchi, P. Renucci, S. Tongay, B. Urbaszek, and X. Marie, "Exciton radiative lifetime in transition metal dichalcogenide monolayers," Phys. Rev. B **93**, 205423 (2016).
[13]S. Ayari, A. Smiri, A. Hichri, S. Jaziri, and T. Amand, "Radiative lifetime of localized excitons in transition-metal dichalcogenides," Phys. Rev. B **98**, 205430 (2018).
[14]A. Wang, X. Wu, S. Zhao, Z. V. Han, Y. Shi, G. Cerullo, and F. Wang, "Electrically tunable non-radiative lifetime in WS_2/WSe_2 heterostructures," Nanoscale **16**, 13687 (2024).

[15]G. Moody, J. Schaibley, and X. Xu, "Exciton dynamics in monolayer transition metal dichalcogenides *invited*," J. Opt. Soc. Am. B **33**, C39–C49 (2016).
[16]T. Kuechle, S. Klimmer, M. Lapteva, T. Hamzayev, A. George, A. Turchanin, T. Fritz, C. Ronning, M. Gruenewald, and G. Soavi, "Tuning exciton recombination rates in doped transition metal dichalcogenides," Opt. Mater.: X **12**, 100097 (2021).
[17]K. F. Mak, C. Lee, J. Hone, J. Shan, and T. F. Heinz, "Atomically thin MoS_2: A new direct-gap semiconductor," Phys. Rev. Lett. **105**, 136805 (2010).
[18]Y. Lin, X. Ling, L. Yu, S. Huang, A. L. Hsu, Y.-H. Lee, J. Kong, M. S. Dresselhaus, and T. Palacios, "Dielectric screening of excitons and trions in single-layer MoS_2," Nano Lett. **14**, 5569–5576 (2014).
[19]G. Wang, A. Chernikov, M. M. Glazov, T. F. Heinz, X. Marie, T. Amand, and B. Urbaszek, "Colloquium: Excitons in atomically thin transition metal dichalcogenides," Rev. Mod. Phys. **90**, 021001 (2018).
[20]E. C. Regan, D. Wang, E. Y. Paik, Y. Zeng, L. Zhang, J. Zhu, A. H. MacDonald, H. Deng, and F. Wang, "Emerging exciton physics in transition metal dichalcogenide heterobilayers," Nat. Rev. Mater. **7**, 778 (2022).
[21]E. L. Peterson, T. I. Andersen, G. Scuri, A. Y. Joe, A. M. Mier Valdivia, X. Liu, A. A. Zibrov, B. Kim, T. Taniguchi, K. Watanabe, J. Hone, V. Walther, H. Park, P. Kim, and M. D. Lukin, "Dynamical control of excitons in atomically thin semiconductors," arXiv:2407.11252 (2024).
[22]A. R. Beattie, P. T. Landsberg, and H. Fröhlich, "Auger effect in semiconductors," Proc. R. Soc. London, Ser. A **249**, 16–29 (1959).
[23]B. Gel'mont, "Three-band Kane model and Auger recombination," Zh. Eksp. Teor. Fiz. **75**, 536 (1978) [JETP **48**, 258 (1978)], http://jetp.ras.ru/cgi-bin/dn/e_048_02_0268.pdf.
[24]A. Haug, "Auger recombination in direct-gap semiconductors: Band-structure effects," J. Phys. C: Solid State Phys. **16**, 4159 (1983).
[25]V. Perebeinos and P. Avouris, "Phonon and electronic nonradiative decay mechanisms of excitons in carbon nanotubes," Phys. Rev. Lett. **101**, 057401 (2008).
[26]K. Bushick and E. Kioupakis, "Phonon-assisted Auger-meitner recombination in silicon from first principles," Phys. Rev. Lett. **131**, 076902 (2023).
[27]D. Li, C. Trovatello, S. Dal Conte, M. Nuß, G. Soavi, G. Wang, A. C. Ferrari, G. Cerullo, and T. Brixner, "Exciton–phonon coupling strength in single-layer $MoSe_2$ at room temperature," Nat. Commun. **12**, 954 (2021).
[28]G. Antonius and S. G. Louie, "Theory of exciton-phonon coupling," Phys. Rev. B **105**, 085111 (2022).
[29]M. Katzer, M. Selig, L. Sigl, M. Troue, J. Figueiredo, J. Kiemle, F. Sigger, U. Wurstbauer, A. W. Holleitner, and A. Knorr, "Exciton-phonon scattering: Competition between the bosonic and fermionic nature of bound electron-hole pairs," Phys. Rev. B **108**, L121102 (2023).
[30]F. Cadiz, E. Courtade, C. Robert, G. Wang, Y. Shen, H. Cai, T. Taniguchi, K. Watanabe, H. Carrere, D. Lagarde, M. Manca, T. Amand, P. Renucci, S. Tongay, X. Marie, and B. Urbaszek, "Excitonic linewidth approaching the homogeneous limit in MoS_2-based van der waals heterostructures," Phys. Rev. X **7**, 021026 (2017).
[31]M. Selig, G. Berghäuser, A. Raja, P. Nagler, C. Schüller, T. F. Heinz, T. Korn, A. Chernikov, E. Malic, and A. Knorr, "Excitonic linewidth and coherence lifetime in monolayer transition metal dichalcogenides," Nat. Commun. **7**, 13279 (2016).
[32]A. Raja, M. Selig, G. Berghäuser, J. Yu, H. M. Hill, A. F. Rigosi, L. E. Brus, A. Knorr, T. F. Heinz, E. Malic, and A. Chernikov, "Enhancement of exciton–phonon scattering from monolayer to bilayer WS_2," Nano Lett. **18**, 6135–6143 (2018).
[33]G. Moody, C. Kavir Dass, K. Hao, C.-H. Chen, L.-J. Li, A. Singh, K. Tran, G. Clark, X. Xu, G. Berghäuser, E. Malic, A. Knorr, and X. Li, "Intrinsic homogeneous linewidth and broadening mechanisms of excitons in monolayer transition metal dichalcogenides," Nat. Commun. **6**, 8315 (2015).
[34]S. Brem, A. Ekman, D. Christiansen, F. Katsch, M. Selig, C. Robert, X. Marie, B. Urbaszek, A. Knorr, and E. Malic, "Phonon-assisted photoluminescence from indirect excitons in monolayers of transition-metal dichalcogenides," Nano Lett. **20**, 2849–2856 (2020).
[35]V. Funk, K. Wagner, E. Wietek, J. D. Ziegler, J. Förste, J. Lindlau, M. Förg, K. Watanabe, T. Taniguchi, A. Chernikov, and A. Högele, "Spectral asymmetry of phonon sideband luminescence in monolayer and bilayer WSe_2," Phys. Rev. Res. **3**, L042019 (2021).
[36]B. Aslan, C. Yule, Y. Yu, Y. J. Lee, T. F. Heinz, L. Cao, and M. L. Brongersma, "Excitons in strained and suspended monolayer WSe_2," 2D Materials **9**, 015002 (2021).
[37]M. Katzer, M. Selig, D. Christiansen, M. V. Ballottin, P. C. M. Christianen, and A. Knorr, "Impact of optically pumped nonequilibrium steady states on luminescence emission of atomically thin semiconductor excitons," Phys. Rev. Lett. **131**, 146201 (2023).
[38]Z. Li, T. Wang, S. Miao, Y. Li, Z. Lu, C. Jin, Z. Lian, Y. Meng, M. Blei, T. Taniguchi, K. Watanabe, S. Tongay, W. Yao, D. Smirnov, C. Zhang, and S.-F. Shi, "Phonon-exciton interactions in WSe_2 under a quantizing magnetic field," Nat. Commun. **11**, 3104 (2020).
[39]Y.-h. Chan, M. H. Naik, J. B. Haber, J. B. Neaton, S. G. Louie, D. Y. Qiu, and F. H. da Jornada, "Exciton–phonon coupling induces a new pathway for ultrafast intralayer-to-interlayer exciton transition and interlayer charge transfer in WS_2–MoS_2 heterostructure: A first-principles study," Nano Lett. **24**, 7972–7978 (2024).
[40]S. Fang, R. Kuate Defo, S. N. Shirodkar, S. Lieu, G. A. Tritsaris, and E. Kaxiras, "Ab initio tight-binding Hamiltonian for transition metal dichalcogenides," Phys. Rev. B **92**, 205108 (2015).
[41]M. Rohlfing and S. G. Louie, "Electron-hole excitations and optical spectra from first principles," Phys. Rev. B **62**, 4927–4944 (2000).
[42]B. Scharf, T. Frank, M. Gmitra, J. Fabian, I. Žutić, and V. Perebeinos, "Excitonic Stark effect in mos_2 monolayers," Phys. Rev. B **94**, 245434 (2016).
[43]L. V. Keldysh, "Coulomb interaction in thin semiconductor and semimetal films," Pis'ma Zh. Eksp. Teor. Fiz. **29**, 716 (1979) [JETP Lett. **29**, 658 (1979)], http://jetpletters.ru/ps/1458/article_22207.shtml.
[44]P. Cudazzo, I. V. Tokatly, and A. Rubio, "Dielectric screening in two-dimensional insulators: Implications for excitonic and impurity states in graphane," Phys. Rev. B **84**, 085406 (2011).
[45]T. C. Berkelbach, M. S. Hybertsen, and D. R. Reichman, "Theory of neutral and charged excitons in monolayer transition metal dichalcogenides," Phys. Rev. B **88**, 045318 (2013).
[46]The relative permittivity in our model is the average value computed from the relative permittivity above and below the TMDC monolayer, for example, $\kappa = (1 + 3.9)/2 = 2.45$ for a TMDC monolayer on top of a SiO_2 substrate (with air above the TMDC monolayer).
[47]Strictly speaking, occupied conduction bands also lead to additional screening of $W(|\boldsymbol{R}|)$, resulting in $W(|\boldsymbol{R}|) \neq V(|\boldsymbol{R}|)$. For simplicity, we neglect this screening in $W(|\boldsymbol{R}|)$. Additional screening due to doping leads to smaller exciton binding energies and to a band gap renormalization, which mostly compensates for the reduction in binding energy. Since we only consider relatively small doping densities, we assume that these effects will not significantly affect the exciton wave function $\mathscr{A}^{Sq}_{vc\boldsymbol{k}}$.